Three-Dimensional Solution of Flows over Wings with Leading-Edge Vortex Separation

James A. Weber,* Guenter W. Brune,* Forrester T. Johnson,†
Paul Lu,‡ and Paul E. Rubbert§
The Boeing Company, Seattle, Wash.

The application of a new, general, potential flow computational technique to the solution of the subsonic, three-dimensional flow over wings with leading-edge vortex separation is presented. The present method is capable of predicting forces, moments, and detailed surface pressures on thin, sharp-edged wings of rather arbitrary planform. The wing geometry is arbitrary in the sense that leading and trailing edges may be curved or kinked and the wing may have arbitrary camber and twist. The method employs an inviscid flow model in which the wing, the rolled-up vortex sheets, and the wake are represented by piecewise continuous quadratic doublet sheet distributions. The Kutta condition is imposed along all wing edges. Strengths of the doubtlet distributions as well as shape and position of the free vortex sheet spirals are computed in iterative fashion, starting with an assumed initial sheet geometry. The method is verified by numerous computed results.

I. Introduction

THE flow at the leading and tip edges of a swept wing with sharp edges separates at moderate to high angles of attack, the separation producing vortex sheets that roll up into strong vortices above the upper surface of the wing. The formation of these vortices is responsible for the well-known nonlinear aerodynamic characteristics exhibited over the angle-of-attack range (Fig. 1).

The leading-edge suction analogy[1,3] provides a method suitable for calculating the magnitude of the nonlinear vortex lift on a rather broad class of wing planforms. Polhamus[1] reasoned that the normal force needed for the flow around a leading edge to reattach to the wing is equivalent to the leading-edge suction force necessary to force the flow to be attached to the leading edge in an unseparated condition. The unseparated leading-edge suction force is calculated and then is rotated normal to the wing to obtain the lift contribution of the leading-edge vortex. The total wing lift computed by this method agrees well with experimental data, but the leading-edge suction analogy does not give flowfield details or detailed surface pressure distributions.

Several attempts have been made in the past toward the theoretical prediction of detailed pressure distributions and flowfields above swept wings with leading-edge vortex separation. Most of these past methods are limited to slender configurations, a considerable simplification, because the problem can be reduced to a solution of Laplace's equation in the crossflow plane, for which conformal mapping becomes a powerful tool. Smith[4] developed the best-known method of this type by improving the work done earlier in collaboration with Mangler.[5] Assuming conical flow, which is approximately valid near the apex of the wing, he was able to predict qualitatively the type of pressure distributions that had been observed experimentally. Those pressure distributions (Fig. 2) exhibit a vortex-induced pressure peak at about 70% of the local semispan of the wing. Toward the trailing edge, Smith's method overpredicts the experimental load distribution by a considerable amount, because his conical theory does not satisfy the Kutta condition at the trailing edge. Figure 2 shows such a comparison of Smith's theory with experiments and also, for illustrative purposes, spanwise pressure distributions from linear lifting-surface theory[6] and from Jones' slender-wing theory[7] at two chordwise stations of a delta wing. This figure (supplied by Blair B. Gloss of NASA-Langley) shows clearly that none of these theories can predict even approximately aerodynamic load distributions of wings with leading-edge vortex separation and demonstrates the need for an accurate prediction method for this type of flow phenomenon.

II. Description of Method

Theoretical Model

Experimental studies[8] of the vortex sheet separating from a slender sharp-edged wing revealed that the rolled-up part of the vortex sheet consists of three regions: an outer, convection-dominated region in which the distance between turns

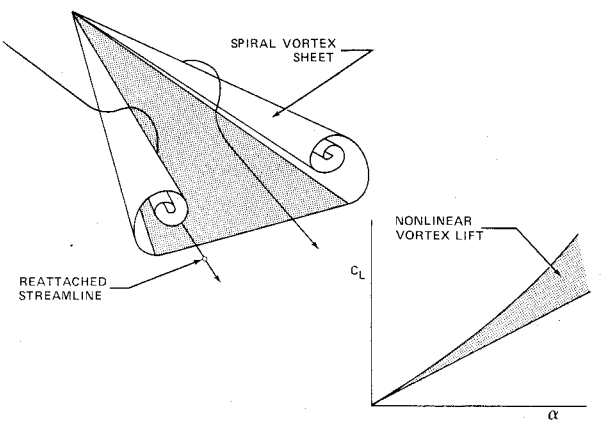

Fig. 1 Leading-edge vortex flow.

Presented as Paper 75-866 at the AIAA 8th Fluid and Plasma Dynamics Conference, Hartford, Conn., June 16-18, 1975; submitted June 25, 1975; revision received Sept. 29, 1975. This work was funded by the NASA Langley Research Center under contract NAS1-12185. The authors wish to thank programer analysts J. Cameron, R. Coleman, and R. Lee of Boeing Computer Services, Inc., for their contributions to this project.

Index categories: Jets, Wakes, and Viscid-Inviscid Flow Interactions; Subsonic and Transonic Flow; Aircraft Aerodynamics (including Component Aerodynamics).

*Specialist Engineer. Member AIAA.
†Senior Specialist Engineer.
‡Specialist Engineer.
§Supervisor, Analytic Methods Group; Senior Group Engineer. Member AIAA.

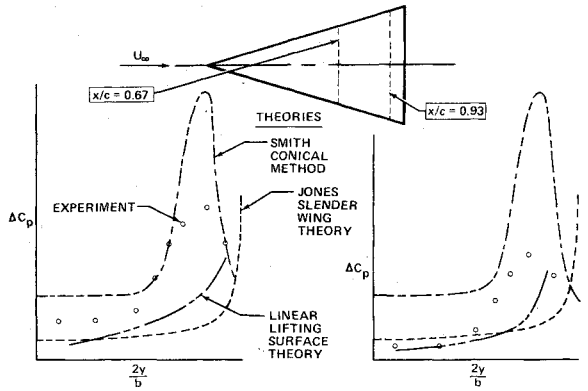

Fig. 2 Load distribution on delta wing given by earlier theories.

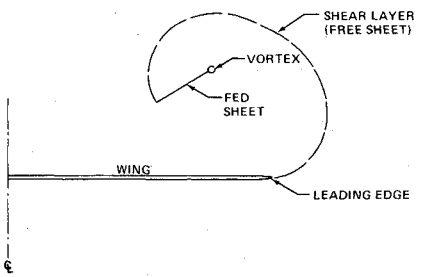

Fig. 3 Smith's leading-edge vortex model.

is large compared to the diffusion distance; an inner region where the distance between turns is of the same order of magnitude as the diffusion distance; and an inner diffusion-dominated viscous core which is very small, representing only about 5% of the vortex diameter. In addition, studies[8,9] of the principal vortex indicate that its shape and strength are relatively independent of Reynolds number. The relative lack of viscosity dependence suggests that the flow may be regarded as potential, with the free shear layer represented either as a vortex sheet or, equivalently, a doublet distribution, supporting a discontinuity in tangential velocity.

A simple method for treating the vortex core was presented by Smith.[4] His model consists of a single vortex with a fed sheet attached to a shear layer springing from the leading edge (Fig. 3). The sheet size and orientation are adjusted so that the total force on the vortex and on the fed sheet is zero. A thorough investigation of mathematical discrete-line vortices revealed that Smith's fed sheet model, when applied to the three-dimensional nonconical flow problem, would contain two self-induced infinite forces,[10] with no possibility of mutual cancellation. The source of the problem with mathematical line vortices is that physical properties of real vortices, featuring a viscous core that prohibits infinite velocities, are ignored.

Hence, a simpler approach for modeling the inner core region was adopted for the present method. The fed sheet is treated as an entirely kinematic extension of the free sheet (Smith's "shear layer"), and no boundary condition is applied to the fed sheet. The assumption in this simplified model is that the boundary conditions applied to the free sheet are sufficient to adequately position the fed sheet, the typical dimension of which is small compared with dimensions associated with the free sheet and with distance from the wing.

The essential elements of the present inviscid and incompressible flow model are the wing, the trailing sheet (wake), the sheet emerging from the wing leading edge and tip (free sheet), and the rolled-up core or spiral region (fed sheet) fed by the leading edge and tip vortex sheets (Fig. 4). The following boundary conditions are imposed on these elements:

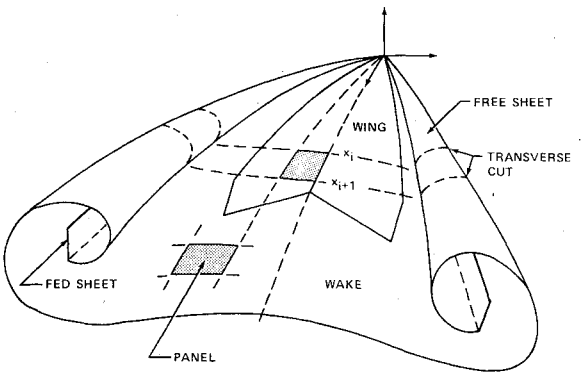

Fig. 4 Geometric description.

1) The flow must be everywhere parallel to the wing surface, that is, $\hat{n}\cdot V^s=0$, where the symbols V^s and $\hat{n}$ are the average velocity (i.e., the average of the velocities on opposing sides of the sheet) and normal vector on the sheet surface, respectively.

2) The free sheet and wake cannot support a pressure differential and must be aligned with the local flow, that is, $\Delta C_p=0$ and $\hat{n}\cdot V^s=0$. (For computational efficiency, a frozen wake is defined which satisfies only the zero pressure jump condition, its position being determined by the upstream elements to which it is attached.)

3) The fed sheet is an entirely kinematic extension of the free sheet, and no boundary conditions are applied to the fed sheet. The size of the fed sheet is chosen by experience or from the conical-flow results of Smith.[4]

4) Kutta conditions are imposed along the leading, side, and trailing edges of the wing in the presence of free sheets emanating from these edges.

The geometric description is that of a general, three-dimensional (not conical) configuration consisting of a thin wing, free sheet, wake, and fed sheet (Fig. 4). The wing geometry is arbitrary in the sense that leading and trailing edges may be curved or kinked and the lifting surface may have arbitrary camber and twist. The configuration is subdivided into a network of quadrilateral panels, the corner points of which are defined by coordinates in transverse cutting planes. The trace of the kinematic fed sheet in a transverse cutting plane is a single planar panel at a fixed angle of approximately 90° to the free sheet.

Basic Concepts and Numerical Procedures

Inviscid, irrotational, incompressible fluid flow is characterized by a perturbation velocity potential ϕ satisfying Laplace's equation

$$\phi_{xx}+\phi_{yy}+\phi_{zz}=0 \tag{1}$$

Compressibility effects over a wide range of subsonic Mach numbers may be approximated by the Goethert rule, in which case a preliminary coordinate transformation again produces Eq. (1). Hence, for the purposes of this paper, only solutions to Eq. (1) are considered.

Green's theorem expresses ϕ, the solution to Eq. (1), in terms of its value and normal derivative on the fluid boundary S:

$$\phi(P)=\int\int_S \frac{\partial\phi(Q)}{\partial n}\left(\frac{-1}{4\pi r}\right)dS + \int\int_S \phi(Q)\frac{\partial}{\partial n}\left(\frac{1}{4\pi r}\right)dS \tag{2}$$

Here r is the distance from the field point P to a boundary surface point Q, and $\partial/\partial n$ is the derivative in the direction of the surface normal $\hat{n}$ pointing into the fluid. Equation (2) gives ϕ as a superposition of a source sheet $\sigma(Q)$ of strength $\partial\phi/\partial n$,

and a doublet sheet $\mu(Q)$ of strength ϕ on the boundary of the fluid. The source and doublet are fundamental solutions of Eq. (1), their strengths being determined by an appropriate set of boundary conditions.

The boundary conditions may be of the Neumann type (specification of $\partial\phi/\partial n$), of the Dirichlet type (specification of ϕ), or of the mixed type. Neumann and Dirichlet boundary-value problems are referred to, respectively, as "analysis" and "design." In the present formulation, all surfaces are considered as "thin," with continuity of $\partial\phi/\partial n$ across the surface, in which case the first term on the right-hand side of Eq. (2) becomes zero and the second term is replaced by an integral over a single side of the surface with $\phi(Q)$ replaced by $\Delta\phi(Q)=\mu(Q)$.

The present method uses a recently developed computational scheme[11] for the numerical solution of Laplace's equation for Neumann, Dirichlet, or mixed boundary-value problems. A boundary-value problem computationally comprises an assemblage of boundary surfaces and their appropriate boundary conditions. A portion of the boundary surface is termed a "network." The boundary surface is discretized into logically independent networks, generally constructed by consideration of the specific characteristics of the physical problem to be solved. Each network consists of a boundary surface oriented arbitrarily in space, composed of source or doublet distributions and accompanied by a properly posed set of analysis (Neumann) or design (Dirichlet) boundary conditions. The computational scheme has been formulated as an aerodynamic influence coefficient method. Essential features of the computational scheme are as follows.

1) Geometry input for a network is a matrix of cornerpoint coordinates. Panel surface shape is obtained by fitting a paraboloid to corner points in an immediate neighborhood by the method of least squares.

2) Discrete values of singularity strength are assigned to certain standard points on each network. A local distribution of surface singularity strength is obtained by fitting a linear source or quadratic doublet form to these discrete values in an immediate neighborhood by the method of least squares.

3) Certain standard points on each network are assigned as control points. These points include panel center points as well as edge abutment downwash points in the case of doublet networks. The latter serve to impose standard aerodynamic edge conditions automatically (for example, the Kutta condition, zero potential jump at thin edges, and continuity of singularity strength across abutting networks), in order to produce logical independence for each network. The number of boundary conditions on each network coincides with the number of assigned surface singularity parameters.

4) Two expansions of the induced velocity kernel are employed. The near-field expansion is based upon the assumption of (relatively) small panel curvature; the far-field expansion is dependent upon a (relatively) large separation distance between the field point and panel. All resultant integrals are evaluated in closed form by means of recursion relations that contain the fundamental logarithm and arc tangent transcendental terms that appear in flat-panel, constant-strength techniques.

Briefly, the following main features of the numerical representation are employed in the present model. Although panel curvature is a feature of the general scheme, within the present model only quadrilateral planar panels are used. They are defined in the near plane determined by neighboring input corner-point coordinates. The wing and free sheet are represented by network distributions of doublets that vary as piecewise continuous quadratic functions in each of two coordinate directions over each panel of the network. The cumbersome shedding of wakes, associated with vortex panels, thus is avoided. An analysis-type network is employed on the wing (geometry of the wing is specified), and a design-type network of doublets simulates the free sheet (unknown free-sheet geometry, zero pressure jump specified). Figures 5 and 6

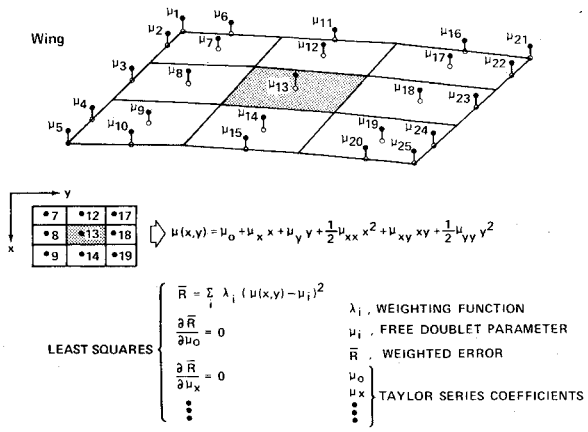

Fig. 5 Analysis network.

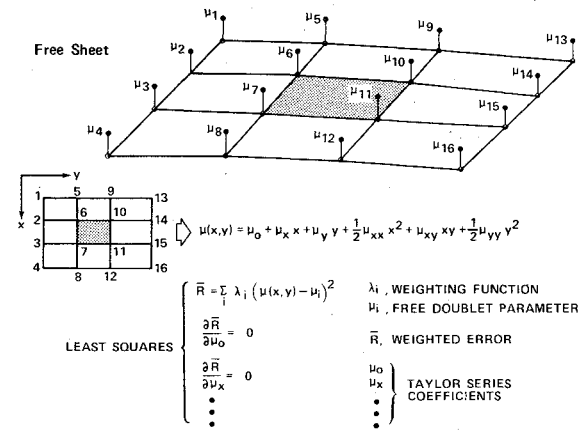

Fig. 6 Design network.

display details of the two networks, showing the arrangements for the free doublet parameters from which the six Taylor's series coefficients of the quadratic panel distributions are determined by least-squares fit. All aerodynamic influence coefficients (AIC) are integrable in closed form, resulting in an efficient and reliable AIC computation. Details of the development of the network formulation and AIC are reported in Ref. 11. Network types used for the wake and fed sheet are specializations of the design-type network.

Solution Procedure

The boundary-value problem of wings with leading-edge vortex separation is nonlinear because the shape of the free vortex sheet, as well as its strength, are unknown. The solution procedure therefore must be iterative. The basic approach driving the iteration involves a small perturbation from an initial guess, which results in a linear formulation for the updated free-sheet position and strength.

The boundary-value problem can be written symbolically in terms of the following three equations:

$$E(\mu_e, \tilde{\mu}, \theta)=0 \tag{3}$$

$$F(\mu_e, \tilde{\mu}, \theta)=0 \tag{4}$$

$$G(\mu_e, \tilde{\mu}, \theta)=0 \tag{5}$$

where those doublet strength parameters defined at certain edge points of networks are denoted by μ_e, all remaining doublet parameters by $\tilde{\mu}$, and the panel geometry by θ, where θ represents the angles of inclination of panel edges in transverse cuts defining the spatial location of free sheet and wake panels. The specific form of these equations is given in Appendix A. Equation (3) expresses the stream surface boundary condition ($\hat{n}\cdot V^s=0$) at certain edge points of networks.

Satisfaction of Eq. (3) is a necessary condition for the satisfaction of the Kutta condition postulated for wing leading and trailing edges. Eq. (4) symbolizes the boundary conditions $\Delta C_p = 0$ of free sheet and wake and $\hat{n} \cdot V^s = 0$ of the wing. Equation (5) is the stream surface boundary condition of the free sheet and wake.

Small perturbations of these equations from an initial "starting solution" result in a set of linear equations governing perturbation variables $\Delta\mu_e$, $\Delta\bar{\mu}$, and $\Delta\theta$. Symbolically,

$$\begin{bmatrix} \partial E/\partial\mu_e & \partial E/\partial\bar{\mu} & 0 \\ \partial F/\partial\mu_e & \partial F/\partial\bar{\mu} & \partial F/\partial\theta \\ \partial G/\partial\mu_e & \partial G/\partial\bar{\mu} & \partial G/\partial\theta \end{bmatrix} \begin{Bmatrix} \Delta\mu_e \\ \Delta\bar{\mu} \\ \Delta\theta \end{Bmatrix} = \begin{Bmatrix} 0 \\ -F \\ -G \end{Bmatrix} \tag{6}$$

where F and G are known and denote the error residual in satisfaction of the boundary conditions at intermediate steps of the iteration cycle.

These equations are solved in each cycle of the iteration procedure to update doublet strength and configuration geometry. Numerical experimentation revealed that it is most advantageous to satisfy Eq. (3) (i.e., the Kutta condition) exactly at every iteration step. It is assumed that the Kutta condition is not affected by the geometry update, i.e., $\partial E/\partial\theta = 0$. To avoid overshooting the correct solution, the step sizes are scaled. Specific details of the iteration scheme are given in Appendix B.

III. Verification of Method

Results

A computer program has been developed to verify the method. The program, which presently is restricted to 125 unknown parameters, is coded for the CDC 6600 computer, occupies 120,000 octal locations of central memory in an overlay structure, and uses eight disk files (the program is also operational on the NASA-Langley CDC 6400 and 6600 computers). Although quotation of execution time is, at best, qualitative because of the many influencing factors, solutions for delta wings have been executed to convergence in under 300 sec of central processor time.

Numerous example cases have been executed to validate the method and its generality. Cases have been selected with a view to comparison with available theoretical and experimental data for a range of different geometric configurations including delta, gothic, and arrow wings. The capability of the method to predict overall wing coefficients is shown in Fig. 7 for a delta wing of aspect ratio 1 at low subsonic speed ($M_\infty = 0$). This figure shows the well-known nonlinear variation of the normal-force coefficient C_N with angle of attack α. Several values of C_N were computed for angles of attack up to 20° and agree well with experimental data of Peckham[9] and theoretical results from the leading-edge suction analogy of Polhamus.[2] The corresponding load distribution at $\alpha = 20°$ is plotted in Fig. 8 and compared with Peckham's experimental results. Although only 25 wing panels were used on one-half of the configuration, the completely three-dimensional nonconical load distribution was predicted well, including the location of the vortex-induced pressure peaks and the decrease of the load toward the trailing edge.

Figures 9-11 show detailed surface pressure distributions for another delta wing of aspect ratio 1.4559 at $\alpha = 8.8°$, $\alpha = 14°$, and $\alpha = 19.1°$. Upper and lower surface pressures are predicted well for the higher angles of attack, as the comparison with experimental data[12] illustrates. At 8.8°, the differences, although unclear, may be due to the blunt trailing edge of the experimental model[12] or to an inadequate definition for the fed sheet geometry. The experimental results clearly show the effect of the secondary vortex separation, which takes place on the upper surface just slightly outboard of the main vortex. The present method does not model secondary vortex separation and, consequently, produces a slightly different shape for the pressure peaks.

The method has application to more general configurations. For example, Fig. 12 shows the method applied to

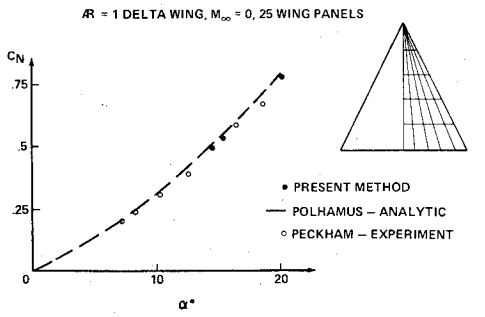

Fig. 7 Normal force coefficient C_N, delta wing.

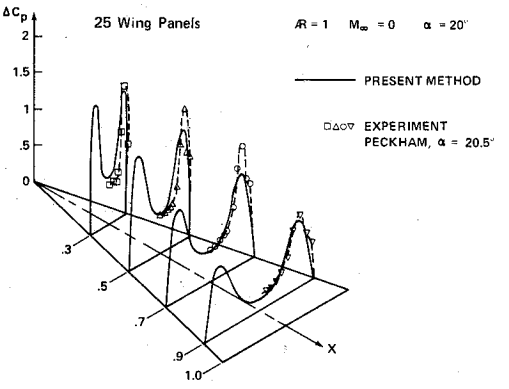

Fig. 8 Load distribution of delta wing with 25 wing panels at $\alpha = 20°$

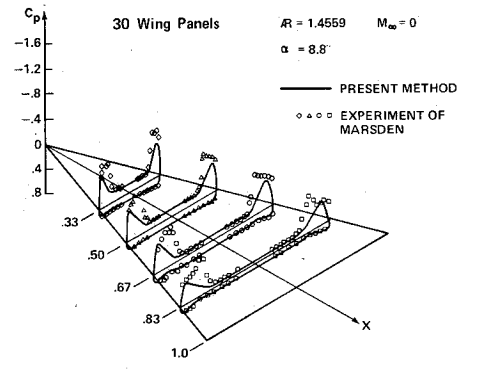

Fig. 9 Surface pressure distribution of delta wing with 30 wing panels at $\alpha = 8.8°$.

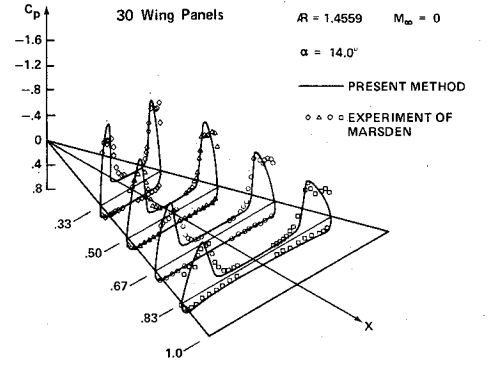

Fig. 10 Surface pressure distribution of delta wing with 30 wing panels at $\alpha = 14.0°$.

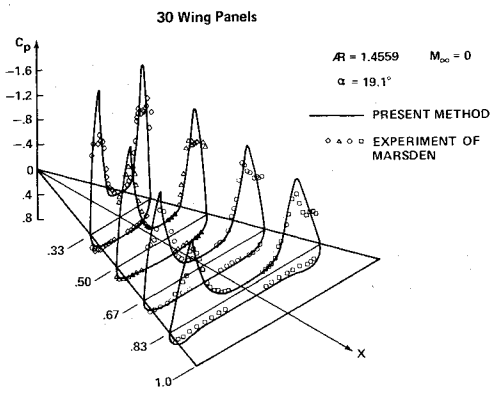

Fig. 11 Surface pressure distribution of delta wing with 30 wing panels at $\alpha = 19.1°$.

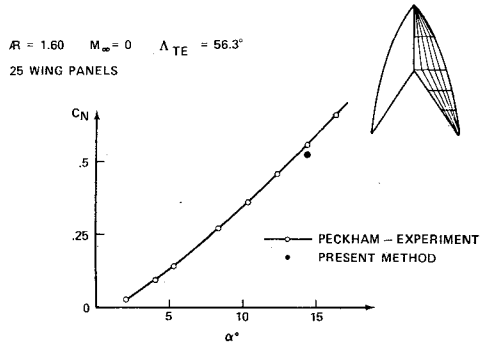

Fig. 12 Normal force coefficient C_N, gothic wing.

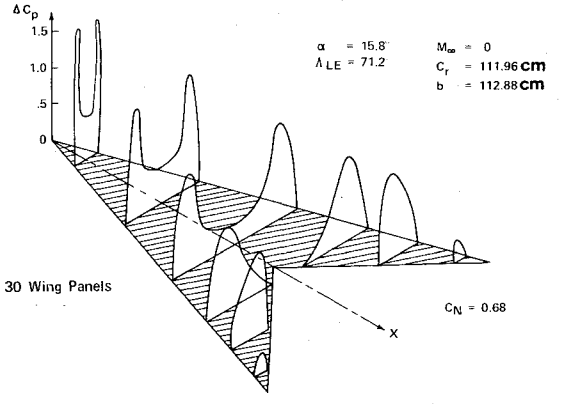

Fig. 13 Load distribution of arrow wing.

a gothic wing having a swept trailing edge and a curved leading edge. This figure shows good agreement of the normal-force coefficient C_N with experiment at the relatively high angle of attack of 14.3°.

Figure 13 shows the predicted load distribution of an arrow wing. Experimental data are not available for comparison, but the plotted loads appear to be realistic and demonstrate that the method is capable of handling other than delta-wing planforms.

Convergence Characteristics

The progress of the solution is monitored by examination of the residual errors in the zero pressure jump boundary condition on the free sheet and wake, and the stream surface boundary condition on the wing [Eq. B9)]. Figure 14 shows the convergence characteristics for a delta wing of aspect ratio 1 and a gothic wing of aspect ratio 1.60. Each configuration has 25 wing panels.

The paneling and convergence characteristics for the delta wing are shown on the left-hand side of Fig. 14, where the normal-force coefficient C_N is shown as a function of

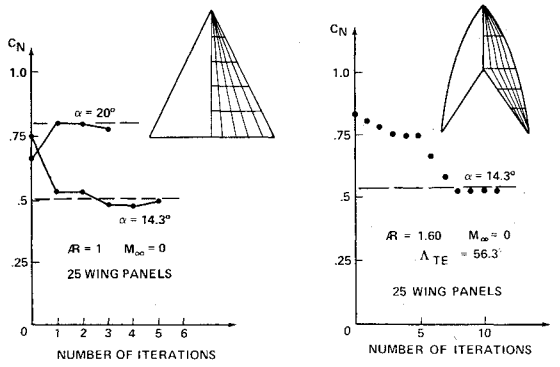

Fig. 14 Convergence characteristics.

iteration number for two different angles of attack. The dashed lines indicate the value of C_N obtained from the leading-edge suction analogy. For this case, the aerodynamic influence coefficients were updated on each cycle of the iteration. The solution quickly seeks a level after only one or two iterations and then exhibits some oscillation, which is often a characteristic of Newton schemes. The paneling and convergence characteristics for the gothic wing are shown on the right-hand side. For this case, the aerodynamic influence coefficients (computation of which consumes the largest fraction of computer run time) were updated only after the fifth and tenth iterations. The difference in convergence characteristics for the two cases is apparent.

IV. Conclusions

The work reported here demonstrates one of the applications of a new, general, subsonic potential flow computational technique recently developed.[11] With the use of this technique, a three-dimensional method has been formulated and verified for predicting the flowfield about swept, sharp-edged wings characterized by the presence of vortex separation at the leading edge. The method has been successful in overcoming the most difficult aspects of the problem and provides the basis for development of this initial capability into a method suitable for supersonic flow and for complete configuration analysis in subsonic and supersonic flow. In addition, it has application to related problems involving free vortex sheets which are encountered in the areas of powered lift, jet interactions, jet flaps, and so forth.

Appendix A: Derivation of Equations

The set of boundary conditions defining the leading-edge vortex problem was represented symbolically in Eqs. (3-5). The derivation of that set is outlined in this Appendix. First, consider several fundamental relationships that hold for a sheet across which a jump in tangential velocity exists (e.g., a doublet sheet). The average velocity for the sheet V^s is given in terms of the upper surface and lower surface velocities V_u and V_l, respectively:

$$V^s = \tfrac{1}{2}(V_u + V_l) \tag{A1}$$

The velocity difference across the sheet V^D is given as

$$V^D = V_u - V_l \tag{A2}$$

The pressure jump ΔC_p across the sheet in incompressible flow is

$$\Delta C_p = (2/|U_\infty|^2)\ (V^s \cdot V^D) \tag{A3}$$

where U_∞ is the freestream velocity.

The jump of tangential velocity across the sheet is created by a doublet distribution μ defined by a set of free doublet parameters μ_p such that $\mu = \mu(\mu_p)$. The sheet velocities are

related directly to μ and μ_p through the local point relationship for V^D and the global matrix relationship for V^s:

$$V^D = \nabla\mu = \nabla\mu(\mu_p) \tag{A4}$$

$$\{V^s\} = [A]\{\mu_p\} \tag{A5}$$

where $[A]$ is the matrix of aerodynamic influence coefficients relating V^s to the doublet parameters μ_p.

The boundary conditions are

Wing

$$\hat{n}\cdot V^s = 0 \tag{A6}$$

Free Sheet and Wake

$$\hat{n}\cdot V^s = 0 \tag{A7}$$

$$\Delta C_p = 0 \tag{A8}$$

plus the Kutta condition, where $\hat{n}$ is the normal vector.

Let the boundary conditions be represented symbolically in terms of the following independent variables: μ_e, doublet strength parameters on the edges of all networks at which the Kutta condition¶ is to be satisfied; $\bar{\mu}$, all remaining doublet strength parameters, and θ, the angles of inclination of panel edges in transverse cuts defining the spatial location of free sheet and wake panels. (Wing networks are spatially fixed.) Equations (A6-A8) are grouped symbolically into the following set:

$$E(\mu_e,\bar{\mu},\theta) \equiv \quad \hat{n}\cdot V^s \quad = 0 \text{ Kutta condition} \tag{A9}$$

$$F(\mu_e,\bar{\mu},\theta) \equiv \begin{cases} \hat{n}\cdot V^s & = 0 \text{ wing} \\ \Delta C_p & = 0 \text{ free sheet and wake} \end{cases} \tag{A10}$$

$$G(\mu_e,\bar{\mu},\theta) \equiv \quad \hat{n}\cdot V^s \quad = 0 \text{ free sheet and wake} \tag{A11}$$

This is a set of nonlinear equations, which is solved by an iterative solution procedure (Appendix B). Starting with an assumed initial solution, the variables μ_e, $\bar{\mu}$, and θ are updated during each cycle of the iteration using a perturbation technique. Consider, for example, Eq. (A9), which can be expanded in a Taylor's series as

$$E^{(i+1)} = E^{(i)} + (\partial E^{(i)}/\partial\mu_e)\Delta\mu_e + (\partial E^{(i)}/\partial\bar{\mu})\Delta\bar{\mu} + (\partial E^{(i)}/\partial\theta)\Delta\theta \tag{A12}$$

where second-order terms of the perturbation variables $\Delta\mu_e$, $\Delta\bar{\mu}$, and $\Delta\theta$ are neglected. The superscript i denotes the ith iteration cycle. Expanding Eqs. (A10) and (A11) in a similar manner and specifying that the boundary conditions are satisfied exactly at the end of the iteration cycle (i.e., $E^{(i+1)} = F^{+1)} = G^{(i+1)} = 0$) results in the following set of linear equations for the perturbation variables for the ith cycle:

$$\begin{bmatrix} \partial E/\partial\mu_e & \partial E/\partial\bar{\mu} & \partial E/\partial\theta \\ \partial F/\partial\mu_e & \partial F/\partial\bar{\mu} & \partial F/\partial\theta \\ \partial G/\partial\mu_e & \partial G/\partial\bar{\mu} & \partial G/\partial\theta \end{bmatrix} \begin{Bmatrix} \Delta\mu_e \\ \Delta\bar{\mu} \\ \Delta\theta \end{Bmatrix} = \begin{Bmatrix} -E \\ -F \\ -G \end{Bmatrix} \tag{A13}$$

¶The Kutta condition is not treated as a separate boundary condition, since by the nature of the free-sheet and wake boundary condition ($\Delta C_p = 0$) it will be satisfied when the solution is achieved. Instead, a smooth "off-flow" condition is imposed as a necessary condition (not sufficient) for the Kutta condition to be satisfied.

where E, F, and G denote the nonzero values of $\hat{n}\cdot V^s$ and ΔC_p remaining after the previous iteration.

The coefficient matrix containing the partial derivatives $\partial E/\partial\mu_e$, $\partial E/\partial\bar{\mu}$ and so forth is known as the Jacobian. For the calculation of the Jacobian, the following assumptions were found to be convenient:

1) Changes of the aerodynamic influence coefficients with respect to changes in geometry are negligible during each cycle of the interation. Periodic updates are performed after a specified number of iterations.

2) $\partial E/\partial\theta = 0$, that is, updating the free sheet geometry by $\Delta\theta$ does not affect the smooth "off-flow" condition at wing edges.

Furthermore, in solving Eq. (A13) for the perturbation variables, the Kutta condition was assumed to be satisfied for each iteration cycle, i.e.,

$$E^{(i)} \equiv 0$$

Appendix B: Iteration Scheme

The perturbation quantities in Eq. (6) are denoted symbolically as ΔX, the coefficient matrix (Jacobian) as J, and the right-hand side as $-f$. Equation (6) becomes

$$J\Delta X = -f \tag{B1}$$

This equation is solved iteratively with a quasi-Newton scheme. Represent the i-th iteration by superscript i. The scheme proceeds to find the corrections $\Delta X^{(i)}$ from the equation

$$J^{(i)}\Delta X^{(i)} = -f^{(i)} \tag{B2}$$

and forms the new approximate solution (termed the next iterate)

$$X^{(i+1)} = X^{(i)} + \delta^{(i)}\Delta X^{(i)} \tag{B3}$$

where $J^{(i)} = J(X^{(i)})$, $f^{(i)} = f(X^{(i)})$, and $\delta^{(i)}$ is a scaling parameter to limit the step size of the correction vector. The Jacobian at $X^{(i+1)}$ is obtained by using the following updata formula[13]:

$$J^{(i+1)} \approx J^{(i)} + D^{(i)} \tag{B4}$$

where

$$D^{(i)} = \frac{\{f^{(i+1)} - f^{(i)} - J^{(i)}\Delta X^{(i)}\}\Delta X^{(i)T}}{\Delta X^{(i)T}\Delta X^{(i)}} \tag{B5}$$

In this way, there is no need to re-evaluate the partial derivatives comprising the elements of the Jacobian at each iteration. The superscript T denotes the transpose of a vector.

Since the aerodynamic influence coefficients form an essential part of the method, the iterative scheme includes a procedure of generating new aerodynamic influence coefficients only after every few iterations. This approach helps to reduce the overall computing costs.

The scaling parameter $\delta^{(i)}$ is introduced to alleviate the problem of overshoot in the classical Newton scheme. For each iteration cycle, the following criteria are used to determine $\delta^{(i)}$:

$$0 < \delta^{(i)} \le 1 \tag{B6}$$

and

$$\delta^{(i)}\|\Delta X^{(i)}\| \le \gamma\|X^{(0)}\| \tag{B7}$$

where γ is a predetermined quantity chosen to limit the length of the correction vector $\delta^{(i)}\Delta X^{(i)}$ to a certain fraction of the

length of the initial vector $X^{(0)}$, and the notation $\| \ \|$ is the Euclidean norm representing the length of a vector. In addition, a halving process of the scaling parameter $\delta^{(i)}$ is applied to insure the inequality

$$\|f^{(i+1)}\| < \|f^{(i)}\| \tag{B8}$$

The quality of the solution is monitored by examination of the residuals defined by

$$R = \sum_k \{ [\Delta(\Delta C_{p\text{sheets}})]^2 + [\Delta(\hat{n} \cdot V^s_{\text{wing}})]^2 \} \tag{B9}$$

where k ranges over all appropriate boundary-condition points.

To initiate the solution process, an initial geometry is required. The size of the fed sheet and the initial free sheet geometry are taken from Smith's conical flow solutions or, as experience allows, by assuming an initial geometry.

References

[1]Polhamus, E.C., "Predictions of Vortex-Lift Characteristics by a Leading-Edge-Suction Analogy," *Journal of Aircraft,* Vol. 8, 1971, p. 193.

[2]Polhamus, E.C., "A Concept of the Vortex Lift of Sharp-Edge Delta Wings Based on a Leading-Edge Suction Analogy, TN D-3767, Dec. 1966, NASA.

[3]Polhamus, E.C., "Application of the Leading-Edge Suction Analogy of Vortex Lift to the Drag-Due-to-Lift of Sharp-Edge Delta Wings," TN D-4739, Aug. 1968, NASA.

[4]Smith, J.H.B., "Improved Calculations of Leading-Edge Separation From Slender Delta Wings," TR66070, March 1966, Royal Aircraft Establishment, Farnborough, Eng.

[5]Mangler, K.W. and Smith, J.H.B., "A Theory of the Flow Past a Slender Delta Wing With Leading-Edge Separation," *Proceedings of the Royal Society,* Vol. 251, May 1959, pp. 200-217.

[6]Lamar, J.E., "A Modified Multhopp Approach for Predicting Lifting Pressures and Camber Shape for Composite Planforms in Subsonic Flow," TN D-4427, July 1968, NASA.

[7]Jones, R.T., "Properties of Low-Aspect-Ratio Pointed Wings at Speeds Below and Above the Speed of Sound," Rept. 835, 1946, NACA.

[8]Maskell, E.C., "Some Recent Developments in the Study of Edge Vortices," *Proceedings of 3rd Congress of the International Council of Aeronautical Sciences,* 1962, Spartan Books, Inc., Washington, D.C., 1964, pp. 737-749.

[9]Peckham, D.H., "Low-Speed Wind-Tunnel Tests on a Series of Uncambered Slender Pointed Wings With Sharp Edges," RM 3186, 1961, British Aeronautical Research Council, London, Eng.

[10]Batchelor, G.K., *An Introduction to Fluid Dynamics,* Cambridge University Press, Cambridge, England, 1967.

[11]Johnson, F.T. and Rubbert, P.E., "Advanced Panel-Type Influence Coefficient Methods Applied to Subsonic Flows," AIAA Paper 75-50, Jan. 1975.

[12]Marsden, D.J., et al, "An Investigation into the Flow over Delta Wings at Low Speeds with Leading-Edge Separation," Rept. 114, ARC 20409, Feb. 1958, The College of Aeronautics, Cranfield, England.

[13]Broyden, C.G., "Quasi-Newton, or Modification Methods," *Numerical Solution of Systems of Nonlinear Algebraic Equations,* edited by G.D. Bryne and C.A. Hall, Academic Press, New York, 1973.

From the AIAA Progress in Astronautics and Aeronautics Series . . .

INSTRUMENTATION FOR AIRBREATHING PROPULSION—v. 34

Edited by Allen Fuhs, Naval Postgraduate School, and Marshall Kingery, Arnold Engineering Development Center

This volume presents thirty-nine studies in advanced instrumentation for turbojet engines, covering measurement and monitoring of internal inlet flow, compressor internal aerodynamics, turbojet, ramjet, and composite combustors, turbines, propulsion controls, and engine condition monitoring. Includes applications of techniques of holography, laser velocimetry, Raman scattering, fluorescence, and ultrasonics, in addition to refinements of existing techniques.

Both inflight and research instrumentation requirements are considered in evaluating what to measure and how to measure it. Critical new parameters for engine controls must be measured with improved instrumentation. Inlet flow monitoring covers transducers, test requirements, dynamic distortion, and advanced instrumentation applications. Compressor studies examine both basic phenomena and dynamic flow, with special monitoring parameters.

Combustor applications review the state-of-the-art, proposing flowfield diagnosis and holography to monitor jets, nozzles, droplets, sprays, and particle combustion. Turbine monitoring, propulsion control sensing and pyrometry, and total engine condition monitoring, with cost factors, conclude the coverage.

547 pp. 6 x 9, illus. $14.00 Mem. $20.00 List

TO ORDER WRITE: Publications Dept., AIAA, 1290 Avenue of the Americas, New York, N. Y. 10019